Biocalcification in porcelaneous foraminifera

Zofia Dubicka[1, 2,3]*, Jarosław Tyszka[4], Agnieszka Pałczyńska[3], Michelle Höhne[1], Jelle Bijma[5], Max Janse[6], Nienke Klerks[6], and Ulf Bickmeyer[1]

[1] *Ecological Chemistry, Alfred-Wegener-Institut Helmholtz-Zentrum für Polar- und Meeresforschung, Bremerhaven D-27570, Germany*

[2]*GFZ German Research Centre for Geosciences, Telegrafenberg, 14473 Potsdam, Germany*

[3]*Faculty of Geology, University of Warsaw, Warsaw PL 02-089, Poland*

[4]*Research Centre in Kraków, Institute of Geological Sciences, Polish Academy of Sciences, Kraków 31-002, Poland*

[5] *Marine Biogeosciences, Alfred-Wegener-Institut Helmholtz-Zentrum für Polar- und Meeresforschung, Bremerhaven D-27570, Germany*

[6]*Burgers' Ocean, Royal Burgers' Zoo, Arnhem 6816 SH, The Netherlands*

*Zofia Dubicka, Faculty of Geology, University of Warsaw, Żwirki i Wigury 93; 02-089 Warsaw, Email: z.dubicka@uw.edu.pl

Keywords: amorphous calcium carbonate, mesocrystals, biomineralization, fluorescence, endosymbiosis, Paleozoic biocalcification, evolution

Abstract

Living organisms control the formation of mineral skeletons and other structures through biomineralization. Major phylogenetic groups usually consistently follow a single biomineralization pathway. Foraminifera, which are very efficient marine calcifiers, making a substantial contribution to global carbonate production and global carbon sequestration, are regarded as the only exception. This phylum has been commonly thought to follow two contrasting models of either "extracellular *in situ* matrix mineralization" attributed to hyaline rotaliid shells, or "intracellular vesicle crystallization" attributed to porcelaneous miliolid shells. Our previous results on rotaliids along with those on miliolids in this paper question such a wide divergence of biomineralization pathways within the same phylum of Foraminifera. We found that both groups produced calcareous shells via the intravesicular formation of unstable mineral precursors (Mg-rich

amorphous calcium carbonate) supplied by endocytosed seawater and deposited *in situ* as mesocrystals formed at the site of new wall formation within the organic matrix. We did not observe calcification of the needles within the transported vesicles, which challenges the previous model of miliolid mineralization. Hence, Foraminifera utilize less divergent crystallization pathways, following the recently discovered biomineralization principles. Mesocrystalline chamber walls are therefore created by accumulating and assembling particles of pre-formed liquid amorphous mineral phase within the extracellular organic matrix enclosed in a biologically controlled privileged space by active pseudopodial structures. Both calcification pathways evolved independently in the Paleozoic and are well-conserved in two clades that represent different chamber formation modes.

Introduction

Over the past 500 million years, living cells have evolved three major skeleton crystallization pathways represented by: (A) mineralization of extracellular matrix; (B) mineralization within a large vesicle; and (C) mineralization within vesicles located in the intracellular space. Very popular in nature is the mineralization of the extracellular matrix (A), for example, in crustacean cuticles, mollusk shells, vertebrate bones, and teeth composed of dentin and enamel (Weiner and Addadi, 2011; Kahil et al., 2021). Radial foraminifera represented by rotaliids have been traditionally interpreted to make use of this crystallization mode (Weiner and Addadi, 2011). The other two pathways (B, C) are both intravesicular and are characterized by either production of amorphous unstable phase within a large vesicle (B), such as a syncytium, well documented for sea urchin larvae (Beniash et al., 1997) or crystallization of calcite elements within smaller vesicles located in the intracellular space (C), as seen in fish that form guanine crystals and coccolithophores to produce coccoliths. This model has also been attributed to the formation of porcelaneous shells by miliolid foraminifera (Weiner and Addadi, 2011) based on the model proposed by Berthold (1976) and followed by Hemleben et al. (1986).

As such, mineralization of shells in Foraminifera is believed to follow two highly contrasting pathways. The current theory states that Miliolida, characterized by imperforate, opaque milky-white shell walls (porcelaneous) (Angell, 1980; Hemleben et al. 1986; de Nooijer et al., 2009), produce fibrillar crystallites composed of Mg-rich calcite within tiny vesicles enclosed by cytoplasm. Miliolid shells are made of randomly distributed needles that cause light reflection, resulting in opaque (porcelaneous) milky walls (Hohenegger, 2009). Calcite needles are thought to be precipitated completely within these vesicles and then transported to the site of chamber formation to be released via exocytosis (Berthold, 1976; Hemleben et al. 1986; Angell, 1980; de Nooijer et al., 2008, 2009). The pre-formed needles or needle stacks are believed to be

continuously embedded in an organic matrix in the shape of the new chamber until the wall is completed. Although this model is commonly accepted, it has never been sufficiently documented *in vivo*, and it does not resolve several conflicting issues. First of all, the question is how pre-formed bundles of parallel calcitic needles are transformed into randomly oriented needles within the shell wall. It is difficult to explain if there is no recrystallization process within the wall structure after discharging the calcite crystallites. This problem was already emphasized by Hemleben et al. (1986). Secondly, why the newly constructed wall is still translucent after deposition of random crystals. We would expect a thin milky opaque layer of the new wall under normal transmitted light, as well as polarized crystals of calcite under crossed nicols. Angell (1980) on his plate 2. presenting chamber formation in *Spiroloculina hyalina* Schulze clearly documented the polarization front being shifted circa a half of the length of the new chamber behind leading edge of the forming chamber. This shift represented more than an hour. Therefore, polarization was missing in the early and middle stage of chamber formation. It means that Angell's (1980) time lapse micrographs of the chamber formation were in conflict with the imaging under TEM. It seems that Angell (1980) was aware of that problem and stressed that calcification had to be "intense enough to show under crossed nicols lags behind the leading edge of the forming chamber" (p. 93, pl. 2 fig. 12/caption). In fact, all experiments that show the "crystal vacuoles" (sensu Angell, 1980) documented under TEM (Berthold, 1976; Hemleben et al. 1986; Angell, 1980) required fixation of the samples, which was prone to post-fixation artifacts of unwanted calcite precipitation.

Our goal is to test whether the miliolid shell is produced by "agglutination" of premade needle-like calcitic crystallites, and in consequence, whether this large group of calcareous Foraminifera follow the third skeleton biomineralization pathway (C) with crystallization within smaller vesicles located in the intracellular space. Therefore, we re-examined the mineralization pathway in Miliolida based on precisely designed experiments on a living species, *Pseudolachlanella eburnea* (d'Orbigny) (Fig. 1). This taxon was selected to facilitate replicated observations of chamber growth under controlled culture conditions.

Our experimental setup excluded TEM imaging to avoid post-fixation artefacts. We included observations of *in vivo* biomineralization using multiphoton and confocal laser scanning microscopy (CLSM) followed by analyses of fixed specimens at different stages of chamber formation by high-resolution field emission scanning electron microscopy (FE-SEM) coupled with energy dispersive X-ray spectrometry (EDS). Our new data challenge of the current understanding of the biomineralization of miliolid foraminifera and such a significant divergence of biomineralization pathways within the Foraminifera.

Results

All replicated *in vivo* experiments on *Pseudolachlanella eburnea* facilitated by CLSM imaging with the application of membrane-impermeable Calcein and FM1-43 membrane dye (performed in separate experiments) showed intravesicular fluorescence signals from a group of moving vesicles (1–5 µm in size) inside the cytosol (Fig. 2, Movies S1 and S2). The fluorescent vesicles inside the cytosol contained seawater, as documented by fluorescence of membrane impermeable Calcein. These vesicles were taken up by endocytosis (FM1-43 staining). The membrane dye (FM1-43) stains the cell membranes and indicates all endocytic vesicles by fluorescence, whereas the other intracellular vesicles remain unstained (Amaral et al., 2011). Both dyes demonstrate the uptake of seawater via the endocytosis of vesicles that are approximately 1–4 µm in diameter and move through the entire cell.

LysoGlow84 experiments revealed the presence of numerous acidic vesicles (Fig. 2, Movies. S3 and S4) inside the cytosol. Acidic vesicles are accompanied by granules (approximately 1–2 µm in size); these show autofluorescence upon excitation at 405 nm (emission 420–480 nm). This characteristic autofluorescence indicates the carbonate content of the vesicles (Fig. S2), which are considered to be Mg-ACCs (amorphous $MgCaCO_3$) (Fig. 2, Movies S4 and S5). Mg-ACC is an unstable, amorphous and hydrated form of $CaCO_3$ with a significantly high concentration of Mg (Raz et al., 2000; Weiner et al., 2003; Bentov and Erez, 2006; Kahil et al., 2021) and is commonly regarded as a resource for most biocalcification processes. Research suggests that a high Mg content not only makes ACC unstable but also facilitates the transport of ACC to the crystallization site, where it is initially transformed into carbonate nanograins (Colfen and Qi, 2001; Addadi and Weiner, 2003; Raz et al., 2003; Dubicka et al., 2023). Carbonate nanograins at the shell construction site were well documented in our SEM-EDS studies (Fig. S6). ACCs have been found in many calcifying marine organisms, such as echinoderms, mollusks, coccolithophorid algae, cyanobacteria, crustaceans, and rotaliid foraminifera, where they are typically interpreted as pre-material phases for the production of calcite skeletons **(**Hasse, et al., 2000; Weiss et al., 2002; Sviben et al., 2016; Dubicka et al., 2018; Kahil et al., 2021).

Symbiont chloroplasts, detected by the typical autofluorescence of chlorophyll (excitation at 405 or 633 nm, emission 650–700, Fig. 2, Movies S3 and S4), have been found to move within the cytosol of the observed specimens, forming mobile clusters with Mg-ACCs and acidic vesicles. Interestingly, endosymbionts were detected only during the mineralization process in specimens with carbonate-bearing vesicles detected by *in vivo* CLSM experiments or just below the organic matrix (OM) of the newly created chamber as seen in FE-SEM observations (Figs. S3G, and S3H).

FE-SEM observations of the fully mineralized test walls display the porcelaneous structures (see Parker, 2017; Dubicka et al., 2018), which are made of three mineralized elements: (a) extrados: outer mineralized surface (approximately 200–300 nm in thickness; Figs. S3C and S4C). (b) Porcelain: the main body of the wall constructed from randomly oriented needle-shaped crystals (up to 1–2 µm in length and approximately 200 nm in width). No organic matter was detected between the needles of the porcelain structures (Figs. 3E; 3E; S4C, and S5A). (c) Intrados: inner mineralized surface (approximately 200–300 nm in thickness) made of needle-shaped elements (Figs. 3E and S5A).

Growing chambers, captured at the various successive stages of chamber formation in different specimens, have revealed the following morphological features: (a) a solitary, thin organic sheath (approximately 200–300 nm thick) that represents the most distal part of the new chamber and is anchored to the older, underlying solid calcified chamber (Fig. 3A); (b) a solitary, outer organic sheath (OOS) filled with spread calcifying nanograins (Figs. 3B; S4A, and S4B); (c) a gel-like OM (4–5 µm in thickness), bounded on two sides by intrados and extrados, and containing relatively widely spaced, randomly dispersed carbonate nanograins (Figs. 3A-B; 4C; S3A-D; S5); (d) the test inside was made of carbonate nanograins that are partly transformed to short needles with a small amount of OM in-between (Figs. 3C, 2D, and 4D); (V) the test inside was composed of needle-shaped crystals with planar faces and without any remaining OM (Figs. 3E and 3E). Both fixation methods (see Material and Methods) yielded highly consistent results. Specimens of *P. eburnea*, which displayed carbonate-bearing vesicles inside the cytosol as determined by CLSM, were fixed using method B, coated with a few nanometers of carbon, and analyzed by SEM-EDS. The main elements detected in the area of the fixed cytoplasm (Fig. S6) were C, O, Na, Mg, P, S, Cl, K, and Ca (of particular interest were the high contents of Mg and Ca), whereas the main elements detected within the area of the new chamber in the form of an organic matrix filled with nanograins (Fig. S6) were C, O, Na, Mg, S, Cl, and Ca. The shell area was strongly enriched with Ca relative to the cytoplasm, which showed a much higher Mg/Ca ratio.

This study shows the lack of premade needle-like crystallites of calcite at the early stages (I-IV) of the wall formation. In contrast, we can clearly infer the *in situ* calcification front with a progressive sequence of crystal growth behind the leading edge of the forming chamber (Figs 4, 5). Therefore, this miliolid species does not produce shells by “agglutination” of premade needle-like crystallites of calcite. In the light of these results, another argument emerges that further confirms in situ calcification of miliolid chambers. It explains the extended transparency of unmineralized walls observed under the light stereomicroscope. The chamber walls under formation tend to gradually change its appearance to milky and opaque aspect during calcification (Fig. 1 E). Our results on biomineralization of this miliolid species do not confirm the formation of

individual skeletal crystallites within intracellular vesicles. However, in turn, our results do support existence of endocytotic vacuolization of sea water in miliolids that first suggested by Hemleben et al. (1986). We further support Angell's (1980) interpretation that the calcite crystals are dispersed in the gel-like organic matrix (see Figs 3A, B; 4C, D; 5). This gel-like fluidal organic matrix most likely include a rich Mg-ACC component as substrate for *in situ* calcification (Figs 3-5).

Discussion

PORCELANEOUS SHELL FORMATION

Comparative analysis of the nanostructures of the newly built chambers combined with the elemental composition obtained from SEM-EDS, as well as data from CLSM, allowed us to identify important steps in the formation of *P. eburnea* shells. The formation of a new chamber begins with the construction of a thin outer organic sheath that pre-shapes the new chamber (Figs. 4, 5). The outer organic sheath is made by pseudopodial structures supported by the cytoskeleton immediately after the extrusion of a small mass of cytoplasm from the aperture (Figs. 1E, and 1F). Once the OOS is constructed, the first calcium carbonate accumulation takes place inside in the form of carbonate nanograins (Figs. S4A and S4B), creating the extrados. The extrados stabilizes the final chamber morphology relatively quickly. Subsequently, the OM gradually thickens and forms the primary accumulation site for the next batches of Mg-rich $CaCO_3$ (hydrated and amorphous). The existence of intracellular, vesicular intermediate amorphous phase (Mg-ACC pools), which supply successive doses of carbonate material to shell production, was supported by autofluorescence (excitation at 405 nm; Fig. 2; Movies S3 and S4; see Dubicka et al., 2023) and a high content of Ca and Mg quantified from the area of cytoplasm by SEM-EDS analysis (Fig. S6). More precise elemental measurements with higher resolution are needed in the future. However, the small size of carbonate-bearing vesicles (approximately 1–2 µm) may make this difficult. Mg^{2+} and Ca^{2+} ions for intracellular production of Mg-ACCs are obtained from seawater and taken up by endocytosis, as independently indicated by membrane impermeable Calcein, as well as by the probe FM1-43 selectively labelling membranes of endocytic vesicles (Figs. 1A and 1B, Movies S1 and S2). We hypothesized that vesicles are carried along cytoskeletal structures to the OM, as observed in Rotaliid foraminifera (Dubicka et al., 2023), where they dock and release their contents (Fig. 4). The nanograins then precipitated within the gelatinous OM, following the release of carbonate from the vesicles (Figs. 3A-C, 4C, and 5). Nanograins filled with OM gradually merge into needle-shaped elements, precipitating *in situ* within the final wall structure (Figs. 3C, 3D, and 4D). The gel-like OM appears to be involved in needle formation; however, the OM seems to disappear (Figs. 3E and 4E) when the needle-shaped crystals are created. We suspect that the OM was removed from the test wall and

recycled by the cell itself. The calcification of extrados and intrados occurs before the interior of the wall crystallizes, providing stability to the new chamber at both edges of the wall (Fig. 3D).

The protruding cytoplasm appears to immediately form a chamber wall by secreting OM and crystals from the vesicles. As calcite secretion continues along the leading edge, the newly formed segment remains covered by a thin, moving sheet of cytoplasm that is called by Angell (1980) the “active sheet”. This thin active sheet of cytoplasm may represent a lamellipodium, that is, a pseudopodial structure involved in the biomineralization of Rotaliida (Tyszka et al., 2019). It is also likely that reticulopodial structures (that do not coat the whole calcification site) are responsible for the distribution and shape of the internal surface of the chamber wall. This occurs by successive accumulation of ACC and OM as identified on TEM images by Angell (1980; p. 97). Results suggest that crystallization of calcite needles is “limited to a confined space controlled by active cytoplasmic structures” and strictly separated by membranes from the cytosol.

FORMATION OF SHELL CRYSTALLITES: A PARADIGM SHIFT

Miliolids were thought to share the same crystallization pathway as coccolith formation in coccolithophorids (Weiner and Addadi, 2011) that evolved in the Triassic, that is c. 210 Myr ago (Gardin et al., 2012). Coccoliths are produced within intracellular Golgi-derived vesicles and then exported to the inner surface of the extracellular coccosphere (de Vrind-de Jong et al., 1986). Miliolids, with their unique fibrillar calcitic microstructures, evolved much earlier, that is ca. 300 Myr ago in the late Paleozoic (Fig. S7). It is generally considered that miliolid crystals also precipitate within vesicles in the cytoplasm and are then transported to the location of the wall construction, where they are released by exocytosis (Berthold, 1976; Angell, 1980; de Noojier et al., 2009; Hemleben et al., 1986; Weiner and Addadi, 2011).

Our results show that needle-shaped crystallites are secreted *in situ* at the area of shell formation within the organic matrix (Figs. 4 and 5), in contrast to the traditional miliolid calcification model (Berthold, 1976; Angell, 1980; Hemleben et al., 1986), in which needle-shaped crystals are initially performed inside the vesicles. Interestingly, the previous studies by Angell (1980) did not support crystal formation within vacuoles either. Precipitation of calcite nanograins, which then merge and transform into crystallites, occurs within the organic matter after the release of Mg^{2+} from Mg-ACC. The organic matter provides an appropriate physiochemical microenvironment for initiating and maintaining the crystallization process by manipulating many essential factors including pH, and kinetics of the system (Kahil et al., 2021). According to Tyszka et al. (Tyszka et al., 2021), the organic matrix involved in the biomineralization of foraminiferal shells may contain collagen-like networks.

Our *in vivo* CLSM observations show a miliolid cytoplasm containing intracellular carbonate-bearing vesicles. Such vesicles have been well-documented by Angell (1980), who stressed their crucial role in the biomineralization process. However, rather than transporting pre-formed solid needles, the vesicles likely carry liquid or quasi-liquid calcification substrates. The liquid phase of the ACC apparently was maintained by a relatively high concentration of Mg (Figs. S2 and S6), which was much higher than that in the shell, as detected by SEM-EDS.

Recently, an independent study was performed on another miliolid species - *Sorites orbiculus* (Nagai et al., 2023). The researchers reported highly complementary results that indicate the lack of crystal-like structures within the intracellular vesicles. Their results suggested that calcification of this miliolid species did not follow Hemleben's et al (1986) model because intracellular vesicles did not produce needle-like crystals to construct the shell wall. They also proposed the need to describe a model of biomineralization in foraminifera.

Because, miliolid wall texture originated together with the appearance of miliolid foraminifera as it has also been recorded within Paleozoic taxa (Fig. S5) thus the calcification mode of miliolids is apparently evolved in the late Paleozoic (≥ 350 Mya) and is well conserved in this clade till today. It should be emphasized that our recent understanding of all calcification pathways in Foraminifera implies their independent evolution within main phylogenetic groups, besides miliolids and rotaliids, also including spirillinids, nodosariids, and robertinids (Mikhalevich, 2004; Pawlowski et al., 2013; Mikhalevich, 2014; Dubicka et al., 2018; Dubicka, 2019; Mikhalevich, 2021; Sierra et al., 2022; de Nooijer et al., 2023). In fact, most of these biomineralization evolutionary transitions from agglutination to calcification originated in the mid and late Paleozoic.

Mg-ACC has also recently been documented in rotaliid foraminifera (Dubicka et al., 2023). Therefore, the biocalcification processes in Rotaliida and Miliolida, which belong to the two main foraminiferal classes Globothalamea and Tubothalamea, respectively (Pawlowski et al., 2013), are more similar than previously thought (Weiner and Addadi, 2011). Their mesocrystalline chamber walls are created by accumulating and assembling particles of pre-formed liquid amorphous mineral phase. Their calcification occurs within the extracellular organic matrix enclosed in a biologically controlled privileged space by active pseudopodial structures. However, we are aware that this process must also vary to some extent as the chemical composition of the calcite, as well as primary crystallite geometries differ between the groups. Seawater provides the relevant Ca and Mg ions for calcification, which are taken up in both groups by endocytosis. In *Amphistegina* (Rotaliida), this process is performed by shell pores (Dubicka et al., 2023), as well as apertures and foramina; in non-porous Miliolida, it is done by granuloreticulopodia emanating from the aperture (Fig. 2, Movie S2). In both the rotaliid *Amphistegina* and the miliolid *P. eburnea* carbonate-bearing vesicles are surrounded by moving acidic vesicles (Fig. 2, Movies S3 and S4),

which likely facilitate pH regulation at the mineralization front (see 28). It is very likely that pH is controlled by active outward proton pumping by a V-type H+ ATPase that is responsible for the proton flux and related calcification (Toyofuku et al., 2017). We suspect much higher pH values within vesicles transporting MgACC to the site of calcification. Such alkaline vesicles were detected by the HPTS fluorescent labelling and reported by several previous studies (de Nooijer et al., 2008; 2009).

Our findings are in line with recent work in biomineralization, supporting that "biominerals grow by the accretion of amorphous particles, which are later transformed into the corresponding mineral phase" (Macías-Sánchez et al., 2011, p. 1; see also Meldun and Cölfen, 2008). Miliolid needles, assembled with calcite nanoparticles, are unique examples of biogenic mesocrystals (see Cölfen and Antonietti, 2005), forming distinct geometric shapes limited by planar crystalline faces. Mesocrystals are constructed from highly ordered individual nanoparticles (Cölfen and Mann, 2003; Strum and Cölfen, 2016; 2017) that form hierarchically structured solid materials in the crystallographic register. These result from the aggregation, self-assembly, and mesoscopic transformation of amorphous precursor nanoparticles. Mesocrystals are common biogenic components in the skeletons of marine organisms, such as corals, echinoderms, bivalves, sea urchins, and rotaliid foraminifera (e.g., Macías-Sánchez et al., 2011; Benzerara et al., 2011; Seto et al., 2012; Evans et al., 2019; Dubicka et al., 2023).

Our biomineralization model further explains the random orientation pattern of the calcite needles within the shell wall. The miliolid intertwined calcitic structure cannot be explained by the models proposed by Berthold (1976) and followed by Hemleben (1986), that is, by the successive deposition of vesicles with ready bundles of solid calcitic fibers (needles) without additional recrystallization processes. In our proposed *in situ* calcification model, calcite crystallites have sufficient space to grow within the flexible gelatinous organic matrix. In addition, our model explains the need for a light and dark phase for the algae that are present inside *P. eburnea* during the biomineralization processes, as these algae possibly play an important role. Small miliolid coiling foraminifera has been regarded as a non-symbiotic taxon because their shells are not transparent, however, this is not true for red and infrared light. Fully developed miliolid shells are made of randomly distributed needles that cause light reflection, resulting in opaque (porcelaneous) walls that possibly protect the foraminifera from UV irradiation and allow them to live in extremely illuminated shallow seas (Hohenegger, 2009). These walls are permeable to red and infrared light, as we observed using multiphoton laser. Red light is commonly believed to be the most efficient waveband for photosynthesis however green light may achieve higher quantum yield of CO_2 assimilation and net CO_2 assimilation rate (Liu and Lerser, 2021). *Pseudolachlanella eburnea* may acquire its facultative symbionts only for the duration of the biomineralization process. The late stage of needle formation in the shell production process ensures that the wall

325 remains transparent by the time the needles are completed. Similar patterns of the gradual
326 change from transparent to opaque whitish walls were also observed in larger symbiotic miliolids
327 by Marshalek (1969), Wetmore (1999), and Tremblin et al. (2022). The latter authors (Tremblin et
328 al., 2022) documented chamber formation of miliolid *Vertebralina striata* with cytoplasm
329 enveloped by a transparent sheath decorated with striate already present in the transparent wall
330 before calcification. They also interpret white areas on the sheath, indicating incipient
331 concentrations of minute calcite crystallites that represent the mineralised wall. The
332 biomineralization process is likely aided by their dark respiratory activity (see Hallock, 1999), as
333 they could supply calcification substrates such as HCO^{3-} through respiration or by increasing pH
334 at the calcification site during the light phase. Similarly, representatives of miliolid large benthic
335 foraminifera (Archaiasidae, Soritidae, and Peneroplidae) host endosymbiotic algae (Lee, 2006;
336 Prazes and Renema, 2019). Therefore, they have developed additional morphological and
337 textural features such as pits, grooves/striate, or windows, which enable light penetration into the
338 places where symbionts are positioned (see Hohenegger, 2009, Parker 2017).
339
340 **Materials and Methods**
341
342 Living foraminifera, collected from the coral reef aquarium in the Burgers Zoo (Arnhem,
343 Netherlands), were cultured in a 10 L aquarium containing seawater with a salinity of 32‰, pH of
344 8.2, and a temperature of 24 °C. *Pseudolachlanella eburnea* (d'Orbigny) was placed in 4 mL petri
345 dishes and observed under a Zeiss Stemi SV8 Stereomikroskope.
346 Selected individuals were studied *in vivo* using a Leica SP5 Confocal Laser Scanning Microscope
347 equipped with an argon, helium-neon, neon, diode, and multiphoton Mai Tai laser (Spectra-
348 Physics) at the Alfred-Wegener-Institut, Bremerhaven, Germany. In *vivo* experiments were
349 performed by labeling samples with different fluorescent dyes (Table 1) just before imaging using,
350 p*H*-sensitive LysoGlow84 (50 µM exc. MP720 nm exc/em. 380–415 nm and 450–470 nm,
351 Marnas Biochemicals Bremerhaven, incubation time: 2 h), FM1-43 membrane stain (1 µM, exc.
352 488 nm em. 580–620 nm, Invitrogen, incubation time: 24 h), and membrane impermeable Calcein
353 (0.7 mg/10 mL, exc. 488 nm, em. 510–555 nm, incubation time: 24 h). The foraminifera were
354 removed from the Petri dish with clean water using a pipette. In addition, the autofluorescence of
355 specific foraminiferal structures at the chosen excitation/emission wavelength was detected. All
356 experiments were replicated with at least several individuals of the same species. All
357 fluorescence probe experiments were performed with appropriate controls.
358 Additional foraminifera individuals that had been studied by CLSM were fixed for further
359 analysis. The fixation process followed two different methods: (A) 60 individuals were transferred
360 to 3% glutaraldehyde for 5 s and then dehydrated stepwise for a few seconds with an
361 ethanol/distilled water mixture with increasing concentrations (30%, 50%, 70%, and 99%). (B)

The seawater was removed from 50 individuals by pipetting and applying a small piece of Kimtech lab wipe (without any rinsing), followed by quick drying in warm air (30–35 °C). This method stops the dissolution of the amorphous mineral phase because there is no contact with other liquids. Fixed foraminifers of both procedures were gently broken using a fine needle to coat the cross-sectional surfaces and tested inside with a few nanometers of either gold or carbon. Foraminifera were then studied using a Zeiss Σigma variable-pressure field-emission scanning electron microscope (VP-FESEM) equipped with EDS at the Faculty of Geology, University of Warsaw.

Acknowledgments

This work was supported by the Alexander von Humboldt Foundation Research Fellowship for experienced researchers (to Z.D.) and the Polish National Science Center (UMO-2018/29/B/ST10/01811) to J.T. and Z.D., a grant coordinated by Grzegorz Racki, University of Silesia. We thank Oscar Branson for his comments on an earlier version of the manuscript and the suggested improvements.

References

Addadi L, Raz S, Weiner S (2003) **Taking advantage of disorder: amorphous calcium carbonate and its roles in biomineralization** *Advanced Materials* **15**: 959–970. https://doi.org/10.1002/adma.200300381

Amaral E, Guatimosim S, Guatimosim C (2018) **Using the fluorescent styryl dye FM1-43 to visualize synaptic vesicles exocytosis and endocytosis in motor nerve terminals** *Methods in Molecular Biology* **689**:137-48. https://doi.org/10.1007/978-1-60761-950-5_8

Angell W (1980) **Test morphogenesis (chamber formation) in the foraminifer *Spiroloculina hyalina* Schulze** *Journal of Foraminiferal Research* **10**: 89–101.

Beniash E, Aizenberg J, Addadi L, Weiner S (1997). **Amorphous calcium carbonate transforms into calcite during sea urchin larval spicule growth** *Proceeding of the Royal Society London B* 264: 461-465. https://doi.org/10.1098/rspb.1997.0066

Bentov S, Erez J (2006) **Impact of biomineralization processes on the Mg content of foraminiferal shells: A biological perspective** *Geochemistry, Geophysics, Geosystems*, **7**. https://doi.org/10.1029/2005GC001015

Benzerara K, Menguy N, Obst M, Stolarski S, Mazur M, Tyliszczak T, Brown GE. Jr, Meibom A (2011) **Study of the crystallographic architecture of corals at the nanoscale by scanning transmission X-ray microscopy and transmission electron microscopy** *Ultramicroscopy* **111**: 1268–1275. 10.1016/j.ultramic.2011.03.023

Berthold WU (1976) **Biomineralisation bei milioliden Foraminiferen und die Matrizen-Hypothese.** *Naturwissenschaften* **63**: 196.

Cölfen H, Qi L (2001) **A systematic examination of the morphogenesis of calcium carbonate in the presence of a double-hydrophilic block copolymer.** *Chemistry–A European Journal* **7**: 106–116.
10.1002/1521-3765(20010105)7:1<106::aid-chem106>3.0.co;2-d

Cölfen H, Antonietti M (2005) **Mesocrystals: Inorganic Superstructures Made by Highly Parallel Crystallization and Controlled Alignment** *Angew. Chem. Int. Ed*. 44: 5576–5591.
10.1002/anie.200500496

Cölfen H, Mann S (2003) **Higher-order organization by mesoscale self-assembly and transformation of hybrid nanostructures**. Angew. Chem. Int. Edit. **42**: 2350–2365.
10.1002/anie.200200562

Hohenegger J (2009) **Functional shell geometry of symbiont-bearing benthic foraminifera** *Galaxea Journal of Coral Reef Studies* **11**: 81–89.
10.3755/galaxea.11.81

Hemleben Ch, Anderson OR, Berthold WU, Spindler M (1986) **Calcification and chamber formation in Foraminifera-A brief overview**, in B.C. Leadbeater and R. Riding (eds.) Biomineralization in Lower Plants and Animals. The Systematics Association, Special vol. 3D, 237–249.

Hu MY, Petersen I, Chang WW, Blurton C, Stumpp M (2020**) Cellular bicarbonate accumulation and vesicular proton transport promote calcification in the sea urchin larva** *Proceedings of the Royal Society B* 287: 20201506.
10.1098/rspb.2020.1506

Debenay, J-P, Guillou J-J, Geslin E, Lesourd M (2000) **Crystallization of calcite in foraminiferal tests** *Micropaleontology* **46**: 87–94.

Dubicka Z, Bojanowski MJ, Bijma J, Bickmeyer U (2022) **Mg-rich amorphous to Mg-low crystalline $CaCO_3$ pathway in foraminifera**. *Heliyon* **9**: e18331
https://doi.org/10.1016/j.heliyon.2023.e18331

Dubicka Z, Owocki K, Gloc M (2018) **Micro- and nanostructures of calcareous foraminiferal tests: insight from some representatives of Miliolida, Rotaliida and Lagenida** *Journal of Foraminiferal Research* **48**: 142–155.
https://doi.org/10.2113/gsjfr.48.2.142

Dubicka Z (2019) **Chamber arrangement versus wall structure in the high-rank phylogenetic classification of Foraminifera.** *Acta Palaeontologica Polonica* **64**: 1-18
doi:https://doi.org/10.4202/app.00564.2018

Erez J (2003) **The source of ions for biomineralization in foraminifera and their implications for paleoceanographic proxies.** *Reviews in Mineralogy and Geochemistry* **54**: 15–149.
https://doi.org/10.2113/0540115.

Evans JS (2019) **Composite Materials Design: Biomineralization Proteins and the Guided Assembly and Organization of Biomineral Nanoparticles** *Materials* **12**: 581. 10.3390/ma12040581

Gardin S, Krystyn L, Richoz S, Bartolini A, Galbrun B (2012) **Where and when the earliest coccolithophores?** *Lethaia* 45: 507–523. https://doi.org/10.1111/j.1502-3931.2012.00311.x

Hallock, P. (1999) **Symbiont-bearing foraminifera** In: Modern foraminifera Springer, Dordrecht. 123–139.

Hasse B, Ehrenberg H, Marxen JC, Becker W, Epple M (2000) **Calcium carbonate modifications in the mineralized shell of the freshwater snail *Biomphalaria glabrata*** *Chemistry–A European Journal* 6: 3679–3685. https://doi.org/10.1002/1521-3765(20001016)6:20<3679::AID-CHEM3679>3.0.CO;2-%23

Kahil K, Weiner S, Addadi L, Gal A (2021) **Ion Pathways in Biomineralization: Perspectives on Uptake, Transport, and Deposition of Calcium, Carbonate, and Phosphate** J. Am. Chem. Soc. **143**: 21100−21112 https://doi.org/10.1021/jacs.1c09174

Kutschera U, Briggs WR (2016) **Phototropic solar tracking in sunflower plants: an integrative perspective** *Annals of Botany* **117**: 1–8. 10.1093/aob/mcv141

Lee JJ (2006) **Algal symbiosis in larger foraminifera** *Symbiosis* **42**:63-75 10.1017/S2475262200002355

Macías-Sánchez E, Willinger MG, Pina CM, Checa AG (2011) **Transformation of ACC into aragonite and the origin of the nanogranular structure of nacre** *Scientific Reports* **7**: 12728. https://www.nature.com/articles/s41598-017-12673-0

Nagai et al., 2023, International Symposium on Foraminifera, FORAMS 2023, Grzybowski Foundation Special Publication, p. 194

Meldrum FC, Cölfen H (2005) **Controlling mineral morphologies and structures in biological and synthetic systems** *Chemical Reviews* **108:** 4332–4432. 10.1021/cr8002856

Mordhorst, T, Awal S, Jordan S, Petters C, Sartoris L, Dringen R, Bickmeyer U (2015) **The chemically synthesized ageladine A-derivative LysoGlow84 stains lysosomes in viable mammalian brain cells and specific structures in the marine flatworm Macrostomum lignano** *Marine Drugs* **13**: 920–935. 10.3390/md13020920

de Nooijer LJ, Toyofuku T, Kitazato H (2009) **Foraminifera promote calcification by elevating their intracellular pH** *Proc. Natl. Acad. Sci. USA* **106**: 15374–15378. 10.1073/pnas.0904306106

de Nooijer LJ, Toyofuku T, Oguri K, Nomaki H, Kitazato,H (2008) **Intracellular pH distribution in foraminifera determined by the fluorescent probe HPTS** *Limnology and Oceanography: Methods* **6**: 610–618.

Parker JH (2017) **Ultrastructure of the test wall in modern porcelaneous foraminifera: implications for the classification of the Miliolida** *Journal of Foraminiferal Research* 47: 136–174.

Pawlowski J, Holzmann M, Tyszka J (2013) **New supraordinal classification of Foraminifera: Molecules meet morphology** *Marine Micropaleontology* 100: 1–10.

Prazeres M., Renema W (2019) **Evolutionary significance of the microbial assemblages of large benthic Foraminifera** *Biological Reviews* 94: 828–848.

Raz S, Weiner S, Addadi L (2003) **Formation of high-magnesian calcites via an amorphous precursor phase: possible biological implications** *Advanced Materials* 12: 38–42.

Raz S, Hamilton PC, Wilt FH, Weiner S, Addadi L (2003) **The transient phase of amorphous calcium carbonate in sea urchin larval spicules: the involvement of proteins and magnesium ions in its formation and stabilization** *Advanced Functional Materials* 13: 480–486.

Seto J, Ma Y, Davis SA, Meldrum F, Gourrier A, Yi-Yeoun K, Schilde U, Sztucki M, Burghammer M, Maltsev S, Jäger C, Cölfen H (2012) **Structure-property relationships of a biological mesocrystal in the adult sea urchin spine** *Proc. Natl. Acad. Sci. USA*, 9, 3699–3704.

Sturm EV, Cölfen H (2016) **Mesocrystals: structural and morphogenetic aspects** Chem. Soc. Rev., 45: 5821.
Sturm EV, Cölfen H (2017) **Mesocrystals: Past, Presence** *Crystals* 7: 207.

Sviben S, Gal A, Hood MA, Bertinetti L, Politi Y, Bennet M, Krishnamoorthy P, Schertel A, Wirth R, Sorrentino A, Pereiro E, Faivre D, Scheffel A (2016) **A vacuole-like compartment concentrates a disordered calcium phase in a key coccolithophorid alga** *Nature Communication* 7: 1–9.

Towe KM, Cifelli R (1967) **Wall ultrastructure in the calcareous foraminifera: crystallographic aspects and a model for calcification**. *Journal of Paleontology* 41, 742–762.

Toyofuku, T., Matsuo, M., de Nooijer, L. et al. (2017) **Proton pumping accompanies calcification in foraminifera** Nature Communication 8, 14145
https://doi.org/10.1038/ncomms14145

Tyszka T, Bickmeyer U, Raitzsch M, Bijma J, Kaczmarek K, Mewes A, Topa P, Janse M (2019) **Form and function of F-actin during biomineralization revealed from live experiments on foraminifera** *Proc. Natl. Acad. Sci. USA* 116: 4111–4116.

Tyszka J, Godos K, Goleń J, Radmacher W (2021) **Foraminiferal organic linings: Functional and phylogenetic challenges** *Earth-Science Reviews* 220: 103726.

de Vrind-de Jong EW, Borman A, Thierry P, Westbroek P, Gruter M, Kamerling JP (1967) Calcification in the coccolithophorids *Emiliania huxleyi* and *Pleurochrysis carterae* II. Biochemical aspects. B.S.C. Leadbeater (Ed.), Biomineralization in Lower Plants and Animals, Clarendon Press, Oxford, 205–217 (1986),

Weiner S, Addadi L (2011) **Crystallization pathways in biomineralization** *Annual Review of Materials Research* 41: 21–40.
https://doi.org/10.1146/annurev-matsci-062910-095803

Weiner S, Levi-Kalisman Y, Raz S, Addadi L (2003) **Biologically formed amorphous calcium carbonate** *Connective Tissue Research* 44, 214–218.

Weiss MI, Tuross N, Addadi L, Weiner S (2002) **Mollusc larval shell formation: amorphous calcium carbonate is a precursor phase for aragonite** *Journal of Experimental Zoology* 293, 478–491.

Table 1. Wavelengths and dyes

dye	concentration	excitation nm	emission nm	source	function
Lysoglow84	50µM	Multiphoton 730	380-415/450-470	Marnas Biochemicals	pH, membrane permeable
FM1-43	1µM	Argon 488 or Multiphoton 1000nm	580-620	Thermo Fisher Scientific	Membrane staining
Calcein	0,7mg/10mL	Argon 488	510-555	Thermo Fisher Scientific	Membrane impermeable water soluble dye
autofluorescence		Diode 405 MP 800	420-490		$CaCO_3$, ACC
autofluorescence		Diode 405/ HeNe 633	650-700		Chlorophyll of symbionts

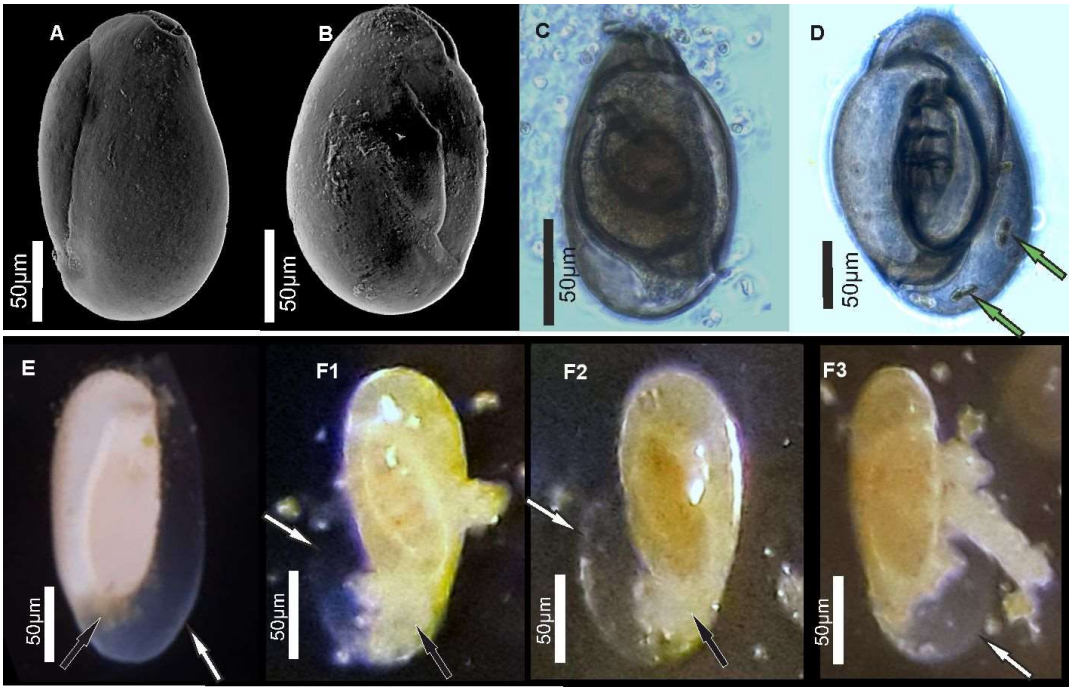

Figure 1. Specimens of miliolid foraminifera, identified as *Pseudolachlanella eburnea* (d'Orbigny), used for experimental studies. (A, B) SEM, (C, D) transmitted light microscope, and (E, F) stereomicroscope images; white arrows show the outer organic sheath of a new chamber during its gradual calcification expressed by its milky, opaque appearance; black arrows show a small mass of cytoplasm extruded from the aperture of exiting the chamber; green arrows show endosymbiotic algae.

585

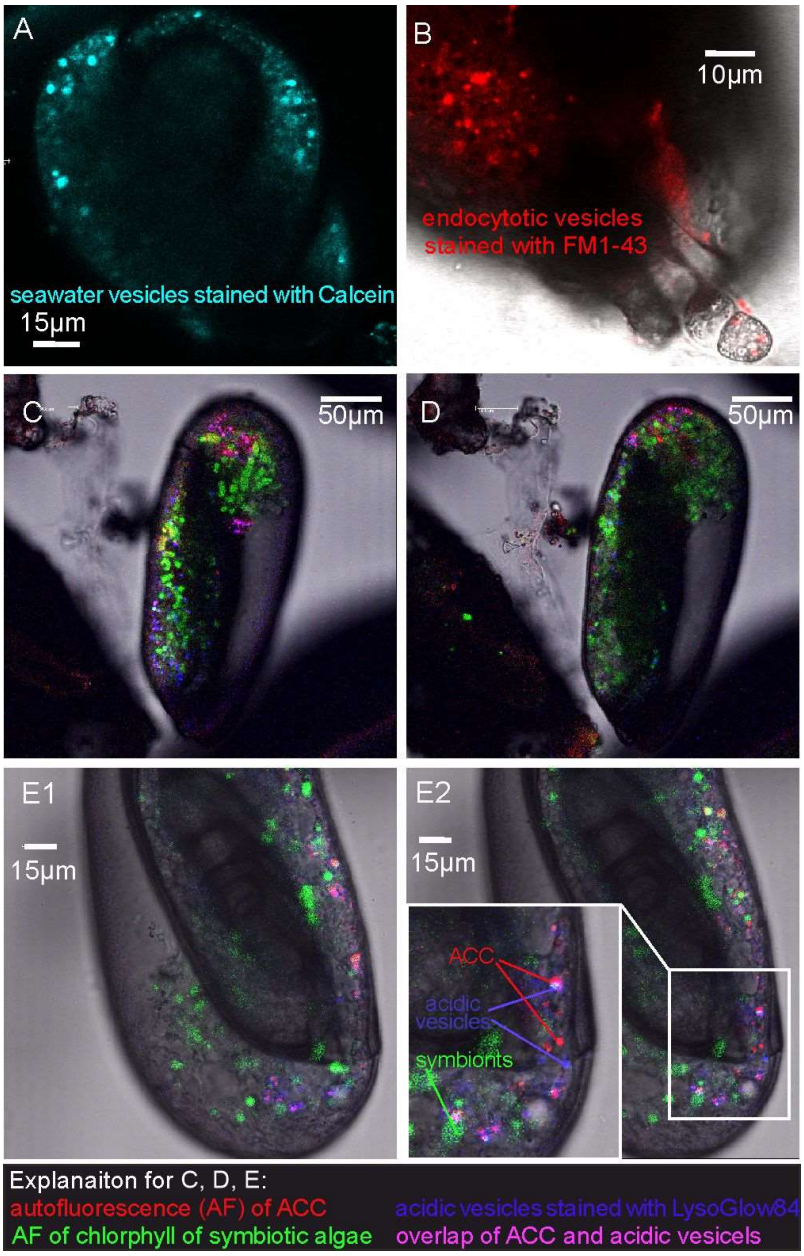

586
587 **Figure 2.** Fluorescence images of living *P. eburnea* conducted by Laser Scanning Microscopy. A
588 - Cell impermeable Calcein (cyan) indicating endocytotic seawater vesicles, see Movie 1. B -
589 FM1-43 membrane dye indicating endocytotic vesicles (red), see Movie 2. C, D, E - LysoGlow84
590 indicating acidic vesicles (navy blue), autofluorescence of chloroplasts (green), and Mg-ACC
591 pools (red), see Movies 3 and 4, (note the overlap of ACC and acidic vesicles is marked in lilac).
592

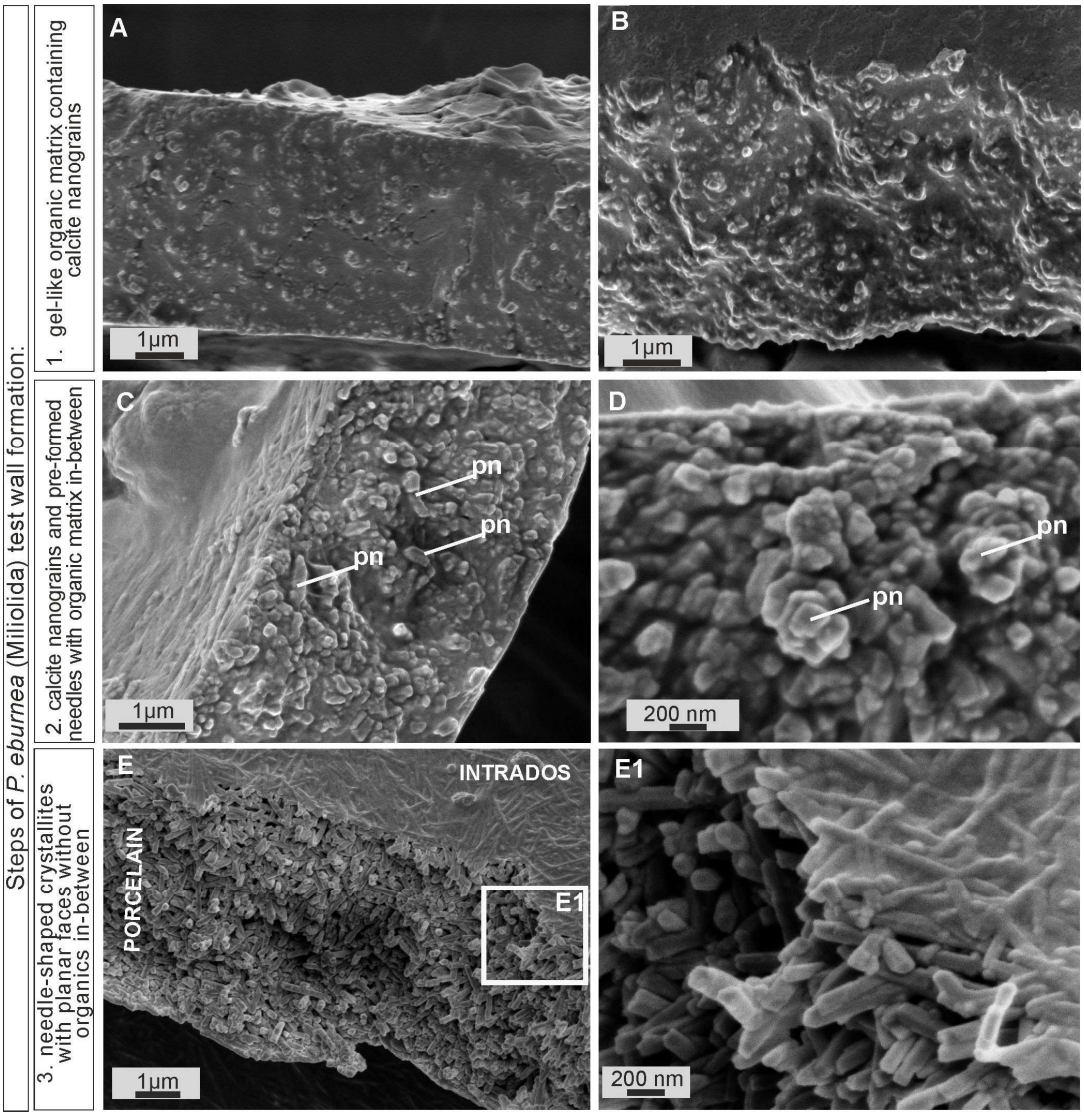

Figure 3. SEM images of the major steps of the formation of *P. eburnea* shell-building components. Test cross-section showing: (A, B) carbonate nanograins within organic matrix, (C, D) nanograins merging into needle-like mesocrystals, (E) fully developed needle-shaped elements; pn –nanograins partly transformed to short needles.

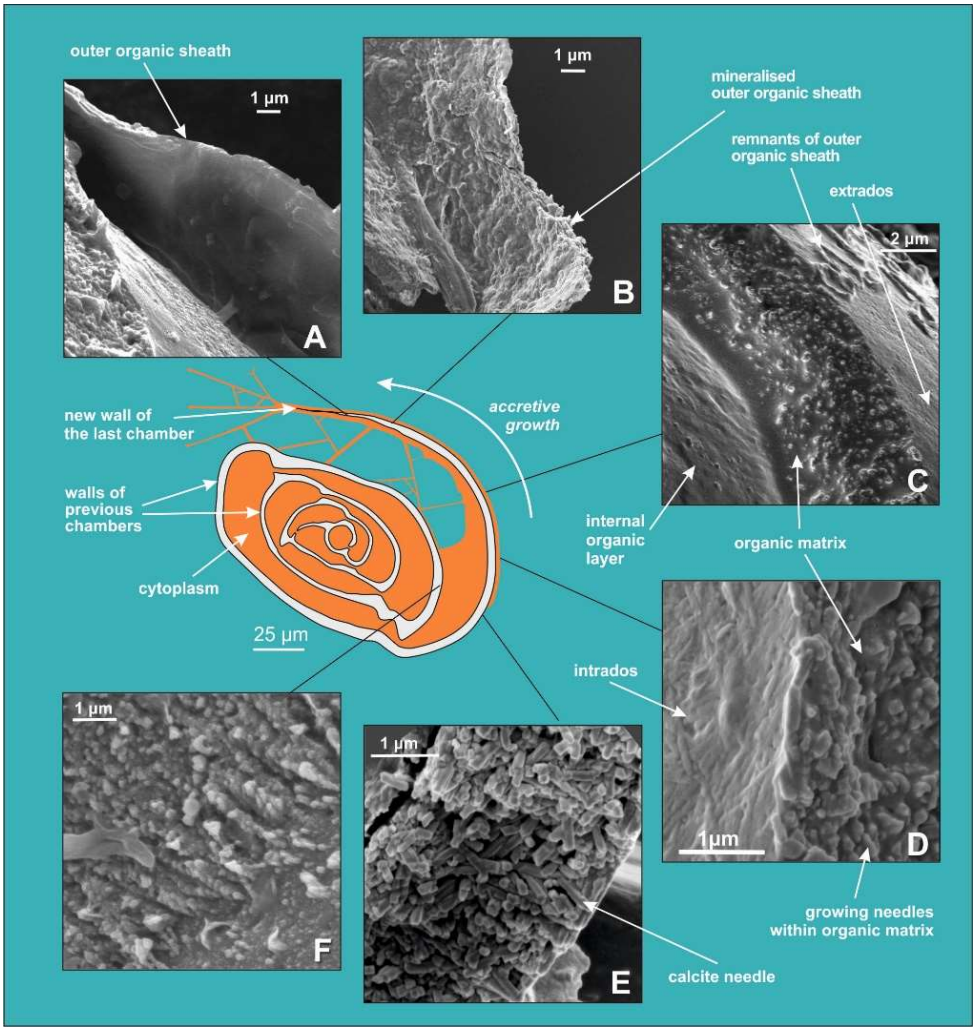

Figure 4. SEM images showing successive stages of new chamber formation in *P. eburnea*. (A) outer organic sheath, (B) mineralized outer organic sheath, (C) calcite nanograins within a gel-like organic matrix, (D) needle-shaped mesocrystal growth, (E) needle-like calcite building elements, (F) nanogranular intrados.

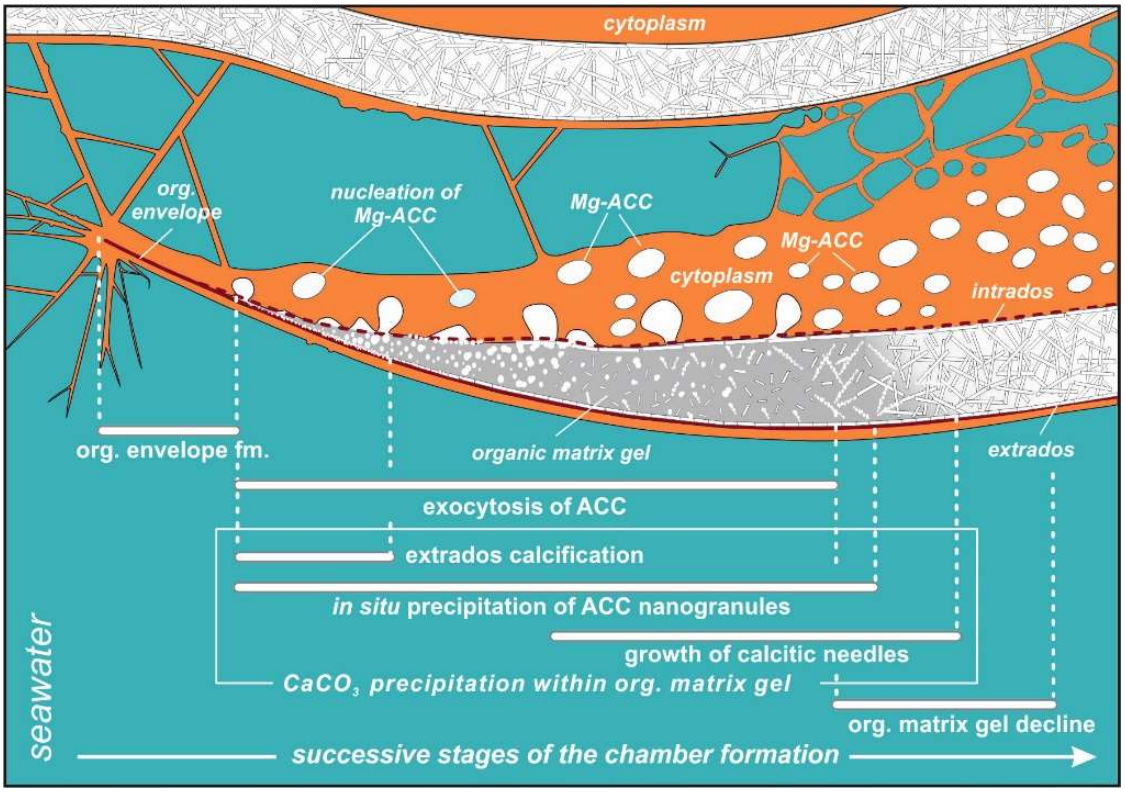

Figure 5. Simplified model of porcelaneous wall construction based on foraminifer *P. eburnea.*

Movie captions

Movie S1 (separate file). Living *P. eburnea* showing cell impermeable Calcein (blue, exc. 488nm em. 505-555) in a series of 107 overlaid images taken during 428 s. Calcein staining indicates the occurrence of seawater vesicles inside the cytosol.

Movie S2 (separate file). FM1-43 membrane probe fluorescent signals (red, exc. 488nm, em. 580-620nm) emitted by intracellular vesicles within cytosol of *P. eburnea.* Because FM1-43 stains only the cell membrane, the observed vesicles must be originated during the process of endocytosis. The movie was taken by overlaid of 84 images during 433 s.

Movie S3 (separate file). Living *P. eburnea* showing fluorescence signal inside the cytosol: autofluorescence of Mg-ACC pools (red, exc. 405nm, em. 420-490nm) and symbiontic chloroplasts (green, exc. 633nm, em. 640-690nm), fluorescent signal of LysoGlow84 pH sensitive

dye (exc. MP 720nm, em. 440-470nm) indicating acidic vesicles. The movie was taken by overlaid of 37 images during 555 s.

Movie S4 (separate file). Living *P. eburnea* showing fluorescence signal inside the cytosol: autofluorescence of Mg-ACC pools (red, exc. 405nm, em. 420-490nm) and symbiontic chloroplasts (green, exc. 633nm, em. 640-690nm), fluorescent signal of LysoGlow84 pH sensitive dye (exc. MP 720nm, em. 440-470nm) indicating acidic vesicles. The movie was taken by overlaid of 37 images during 555 s.